Bull. Chem. Soc. Ethiop. **2024**, 38(6), 1569-1581.
DOI: https://dx.doi.org/10.4314/bcse.v38i6.6

ISSN 1011-3924
Printed in Ethiopia
Online ISSN 1726-801X

TMAB MODIFIED $NIFE_2O_4$ NANOPARTICLES FOR THE EFFECTIVE REMOVAL OF ERIOCHROME BLACK-T AZO DYE

G. Jayanthi[1,2], V. Andal[2*], M. Prabaharan[3] and Suba Kannaiyan[4]

[1]Department of Research, Hindustan Institute of Technology and Science, Padur, Chennai 603103, India
[2]Department of Chemistry, KCG College of Technology, Chennai 600 100, India
[3]Department of Chemistry, Hindustan Institute of Technology and Science, Padur, Chennai 603103, India
[4]Department of Chemistry, Sri Sairam Engineering College, Sai Leo Nagar, West Tambaram, Chennai 600044, India

(Received February 19, 2024; Revised June 20, 2024; Accepted August 2, 2024)

ABSTRACT. The Eriochrome Black-T (EBT) azo dye was removed from aqueous solution using TMAB (tetramethyl ammonium bromide) stabilised $NiFe_2O_4$ (TMAB@NFO) nanoparticles, which have been synthesized through polymeric precursor method. X-ray diffraction (XRD), scanning electron microscopy (SEM), and Fourier transform infrared spectra (FTIR) were used to analyse the TMAB@NFO nanoparticles. Adsorption studies were conducted under a variety of conditions, including pH, adsorbent dosage, and contact time, intraparticle diffusion, pseudo-first- and pseudo-second-order kinetic models were used to analyse the kinetic data. According to the systematic study of adsorption isotherms and kinetics models, TMAB@NFO nanoparticles will adsorb EBT dye utilising the Freundlich model and pseudo-second-order kinetics. The intraparticle diffusion model revealed a linear relationship (R^2 - 0.98, 0.97, and 0.94 for TMAB@$NiFe_2O_4$ and bare $NiFe_2O_4$-NPs), demonstrating how surface modification influences the overall EBT adsorption process and the pore diffusion rate. Additionally, the manufactured nano adsorbents of $NiFe_2O_4$ were effectively regenerated and reused after the treatments up to four times following the elimination of 89% of EBT dye by TMAB@$NiFe_2O_4$-NPs. The results have demonstrated the enormous potential of TMAB @$NiFe_2O_4$-NPs to eliminate EBT in a practical way.

KEY WORDS: Tetramethyl ammonium bromide, $NiFe_2O_4$, EBT, Surface capping, Adsorption, Kinetics

INTRODUCTION

One of the important groups of contaminants from the textile, dyeing, and other industrial processes that are discharged into environment is organic dyes. Therefore, before being released into the environment, the dyes must be removed or degraded. Anionic, cationic, and non-ionic dyes are the three categories. The removal of anionic dyes is thought to be the most difficult task because they are water soluble and produce extremely vivid colours in water with acidic qualities [1, 2].

About 70% of the synthetic dyes used for dyeing purposes by industries worldwide are azo dyes (-N=N-) [3]. After pre-treating silk, wool, and nylon multifibre with chromium salts, the anionic dye EBT, which contains an azo group, is used in the textile industry to color the materials. EBT has a high resistance to light, heat, water, chemical, and microbial attack, making it difficult to degrade even at low concentration levels [4, 5]. It was chosen as an anionic dye for adsorption studies due to its toxicity.

There are numerous physical, chemical, and biological techniques, including reverse osmosis, ultra-filtration, flocculation, adsorption, zonation, precipitation and biodegradation have all been employed for the removal of dyes from the effluent [6-8]. Above mentioned, conventional methods come with a heavy cost and numerous of drawbacks. However, due to its high efficiency, ease of use, and accessibility to a wide variety of adsorbents, the adsorption method is relatively

*Corresponding authors. E-mail: andal.che@kcgcollege.com

widely used [6-10]. Adsorbents in smaller sizes will have greater surface areas and thus greater adsorption capacities. But once saturation adsorption occurs, it becomes challenging to extract the adsorbents from the water. In order to overcome the above problem, currently magnetic nanoparticles are considered to be alternative [7, 9, 11].

Spinel ferrites are magnetic nanoparticles that have a wide range of applications because of their distinct characteristics. Their properties are dependent on their shape, size, synthesis techniques, and surface capping agents. When compared to other spinel ferrites, nano nickel ferrite is the most suited due to its high saturation magnetization and strong chemical and electrochemical stability, which make it an ideal adsorbent [12, 13]. The nanoparticle synthesis process is essential for controlling and modifying the size and shape of the particles. Numerous techniques, including the hydrothermal method [14, 15], microwave method [16], co-precipitation method [17], sol-gel method [18], combustion method [19], green synthesis [20], sonochemical method [21], and modified Pechini process [22], have been used to create nickel ferrite nanoparticles. However, these methods have drawbacks, such as lengthy syntheses times and equipment requirements or uncommon reactants. Thus, we synthesize $NiFe_2O_4$ nanoparticle using polymer (alginic acid) as a gelling agent and stabilized using surfactant tetramethyl ammonium bromide. Tetra methyl ammonium bromide is a quaternary ammonium salt usually such salts have been shown to be capable of stabilising a variety of metal nanoparticles [21-23]. Metal oxide nanoparticles are stabilised for the first time using quaternary ammonium salt (TMAB) through steric and electrostatic interactions [24-28].

There are not many publications on $NiFe_2O_4$ nanoparticles' ability to remove EBT dye. $NiFe_2O_4$ nanoparticles were employed by Moeinpour *et al.* to remove EBT dye, and they observed that pH 6 had the greatest adsorption [29]. Recently, Tahar studied the removal efficiency of EBT using three mixed NiZn ferrite nanoparticles [30]. Hence, for the first time, we used tetra methyl ammonium bromide surfactant to modify $NiFe_2O_4$ nanoparticles.

This study aims to prepare TMAB@$NiFe_2O_4$ nanoparticles utilising alginic acid. The effectiveness of the synthesized nanoparticles to remove EBT dye and their kinetics and mechanism were studied. The Graphical image representing the entire process is enclosed in Figure 1.

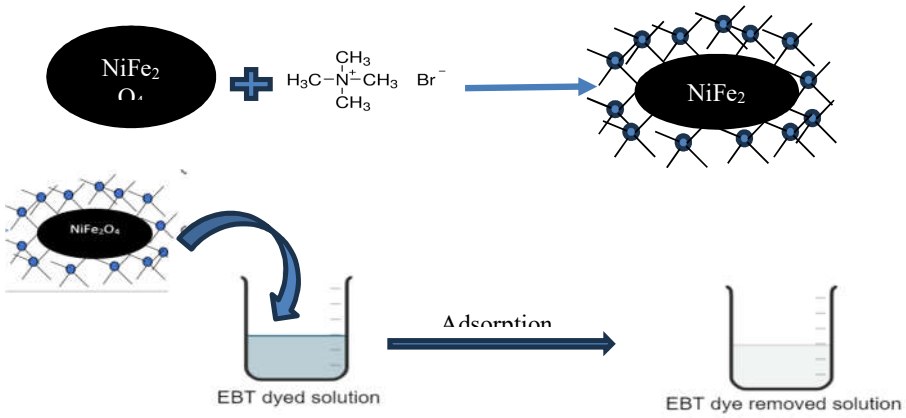

Figure 1. Graphical image representing the entire process.

EXPERIMENTAL

Chemicals

Without additional purification, the compounds nickel nitrate [$Ni(NO_3)_2.6H_2O$], ferric nitrate [$Fe(NO_3)_3.9H_2O$], ammonium hydroxide (NH_4OH), alginic acid and tetramethyl ammonium bromide (TMAB) were utilised after being acquired from SD Fine Chem Limited, Mumbai. Throughout the experiments, double-distilled water was used.

Instruments

Powder X-ray diffraction by (CuK, PAnalytical,) SEM by JEOL 3010, and Fourier transform infrared spectroscopy (FTIR) by a PerkinElmer Frontier spectrophotometer between the ranges of 4000–400 cm^{-1} were used to characterise the produced TMAB @$NiFe_2O_4$.

Preparation of TMAB@$NiFe_2O_4$ nanoparticles

$NiFe_2O_4$ nanoparticles were synthesized by polymeric precursor method. Using a magnetic stirrer, 100 mL of solutions of nickel nitrate (1 M) and ferric nitrate (1 M) were prepared and mixed in a 1:2 [Ni:Fe] ratio. Subsequently, the homogenous solution was gradually added drop by drop into the 5% alginic acid solution (100 mL). Alginic acid is a hetero biopolymer which is water soluble and complexes with cations due to its carbonyl groups. Due to its ionotropic gelling capacity, it is used for synthesis of metal nanostructures [31-33]. Typically, alginic acid coordinates and chelates cations to create an egg box during the gelation process. After that, the resultant gel was dried at 80 ºC for 12 hours. The dry material was calcined between 200 and 700 ºC, with a heating rate of 10 ºC per minute. The synthesized $NiFe_2O_4$ NPs are formed according to the suggested reaction in equation (1) .

$$Ni(NO_3)_2 6H_2O + 2Fe(NO_3)_3.9H_2O \rightarrow NiFe_2O_4 + 8HNO_3 + 20H_2O \quad (1)$$

Then, $NiFe_2O_4$ NPs that had been produced were modified using cationic surfactant (TMAB). 1 g of $NiFe_2O_4$ NPs was added to a 1% TMAB solution, which was then agitated with a mechanical stirrer for 5 hours at 200 rpm. The excess TMAB, which did not react with the $NiFe_2O_4$, was then removed by washing with distilled water. A magnet was used to separate the modified $NiFe_2O_4$ NPs ($NiFe_2O_4$@ TMAB), which was then dried for 24 hours at room temperature.

Adsorption experiments

A series of batch experiments were carried out to analyse the efficiency of TMAB@$NiFe_2O_4$ NPs towards the removal of EBT dye. The experiments were carried out at various parameters such as adsorbent dosage (0.01-0.3 mg), contact time (50-130 min), pH (2-9), dye concentration (10-110 mg/L), and temperature (30-90 ºC). The dye solution containing the NPs was stirred for a predetermined time, and then aliquots were taken and examined with a UV-Vis spectrophotometer. All the experiments were carried out using a mechanical stirrer and a 250 mL beaker with 0.05 g/L of adsorbent and 100 mL of dye solution at room temperature (25 ± 2 ºC) (250 rpm). Experiments on batch adsorption were carried out twice. The following equation was used to determine the TMAB @ $NiFe_2O_4$ NPs' adsorption capacity (mg/g) for EBT removal:

$$E(\%) = \frac{(C_0 - C_t) \times 100}{C_0} \quad (2)$$

where E(%), C_0 and C_t are the dye removal efficiency, initial dye concentration (mg/L) and dye concentration after time t, respectively.

Isotherm studies

The experiments for the isotherm studies were carried out with 100 mL of EBT dye solution and 0.05 g NPs. For 30 min, the respective flasks were agitated at 350 rpm at a temperature of 25 °C. The Langmuir, Freundlich and Temkin, isotherm models were used to further evaluate the adsorption mechanism.

Kinetic studies

The kinetic experiments for EBT dye removal were evaluated using the adsorbent dose (0.05 g). With the help of the pseudo-first order and pseudo-second-order models, the adsorption capacity (qe) was estimated. To characterise the movement of the solid (NPs) and disseminated substance, the intraparticle diffusion kinetic model was applied.

RESULTS AND DISCUSSION

Characterisation of TMAB@$NiFe_2O_4$ nanoparticles

The XRD patterns of the TMAB modified $NiFe_2O_4$ are illustrated in Figure 2. The main characteristic peaks of the synthesised nanoparticles are seen in the XRD data, which were indexed using the JCPDS (10-0325) and showed that nanoparticles were effectively synthesised without any other impurity phases. The XRD pattern of TMAB@$NiFe_2O_4$ shows no different characteristics diffraction peaks in the spectrum, but the intensity was decreased, which may have been due to the surfactants' impact in fine-tuning the nanoparticles' grain sizes [34].

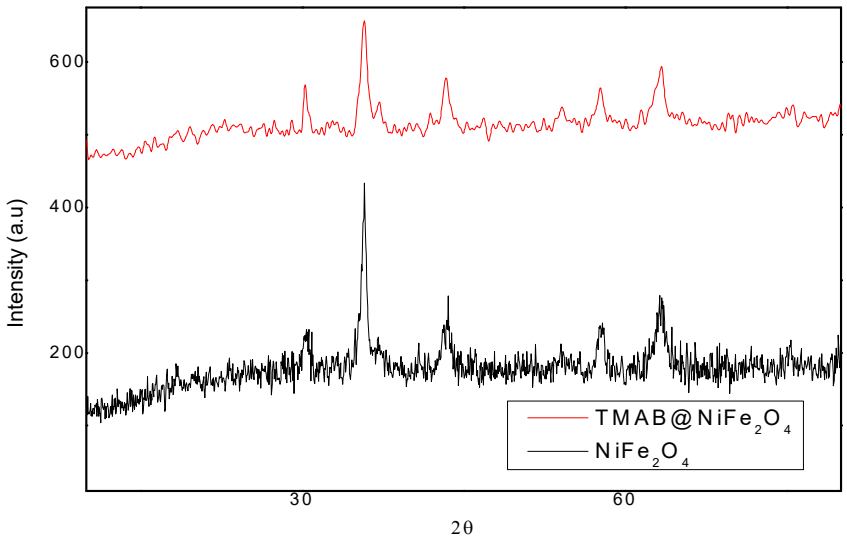

Figure 2. XRD spectra of unmodified and TMAB modified $NiFe_2O_4$ nanoparticles.

Figure 3 shows the SEM images of $NiFe_2O_4$NPs and TMAB@ $NiFe_2O_4$ NPs. The SEM image demonstrates that agglomeration takes place prior to treatment, reducing the surface area of the adsorbent and resulting in less adsorption behaviour. In contrast, the TMAB@$NiFe_2O_4$ NPs are

distributed evenly because the TMAB was capped, preventing agglomeration, size is also reduced, and the surface area was increased, resulting in good adsorption.

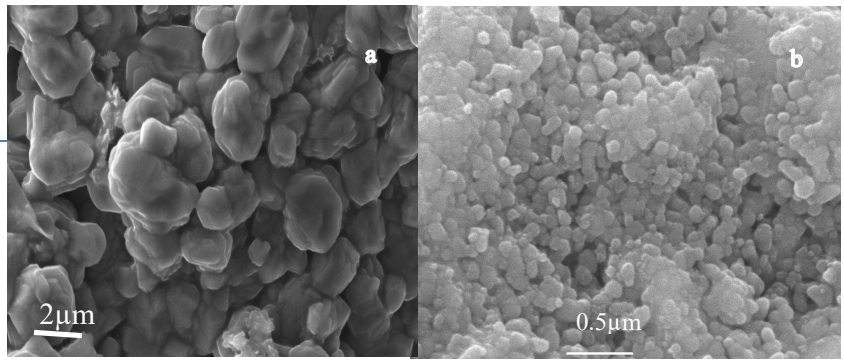

Figure 3. SEM image of (a) unmodified and (b) TMAB modified $NiFe_2O_4$ nanoparticles.

The FTIR analysis of $NiFe_2O_4$ and TMAB@ $NiFe_2O_4$NPs are shown in Figure 4. Both $NiFe_2O_4$NPs and TMAB@$NiFe_2O_4$ have a symmetric vibration of the -OH groups at a wavelength of 3422 cm^{-1}. Observed at 604 cm^{-1} and 463 cm^{-1} are the two main metal-oxygen bands for $NiFe_2O_4$NPs. TMAB modification of the nanoparticles, however, resulted in a small shift in the peaks from 604 to 594 cm^{-1} and 463 to 414 cm^{-1}. This provides as substantive evidence that TMAB modified the nanoparticles [35].

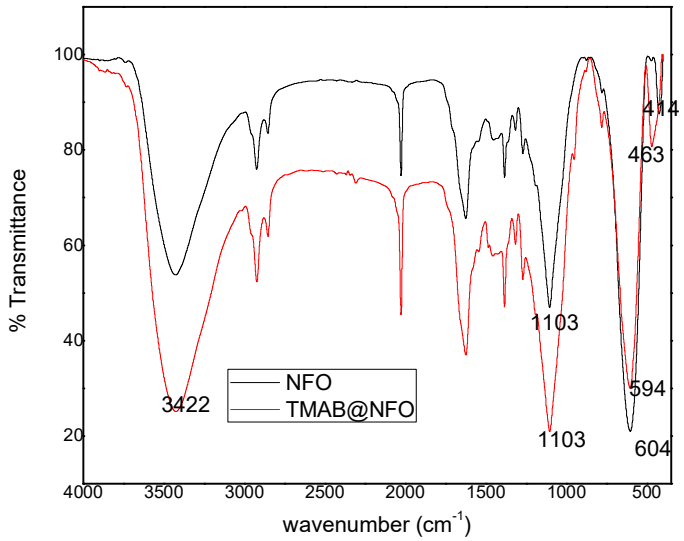

Figure 4. FT-IR spectra of unmodified and TMAB modified $NiFe_2O_4$ nanoparticles.

Adsorption studies on removal of EBT dye by $NiFe_2O_4$ and TMAB@$NiFe_2O_4$

Effect of adsorbent dosage

The adsorptive removal percentage of EBT by TMAB modified and unmodified $NiFe_2O4$ NPs was investigated at various adsorbent dosages between 0.01 and 0.3 mg, with a dye concentration of 10 mg/L, and at pH 6.5. The percentage of EBT removed was closely correlated with the increasing NPs dosage. On increasing the adsorbent dosage from 0.01 mg to 0.07 mg of TMAB@$NiFe_2O_4$ NPs increase in the percentage of dye removal was noticed. A higher percentage of 90% was achieved at 0.07 mg upon further increasing to 0.3 mg a slight increment was noticed. This is explained by the improvement in available adsorbent sites brought on by increased NP dosage.

Nevertheless, unmodified $NiFe_2O_4$ NPs showed a decreased EBT dye removal percentage. The differences in surface area of the synthesized NPs are linked to these persistent discrepancies in the dye adsorption behaviour (Figure 5a) [36].

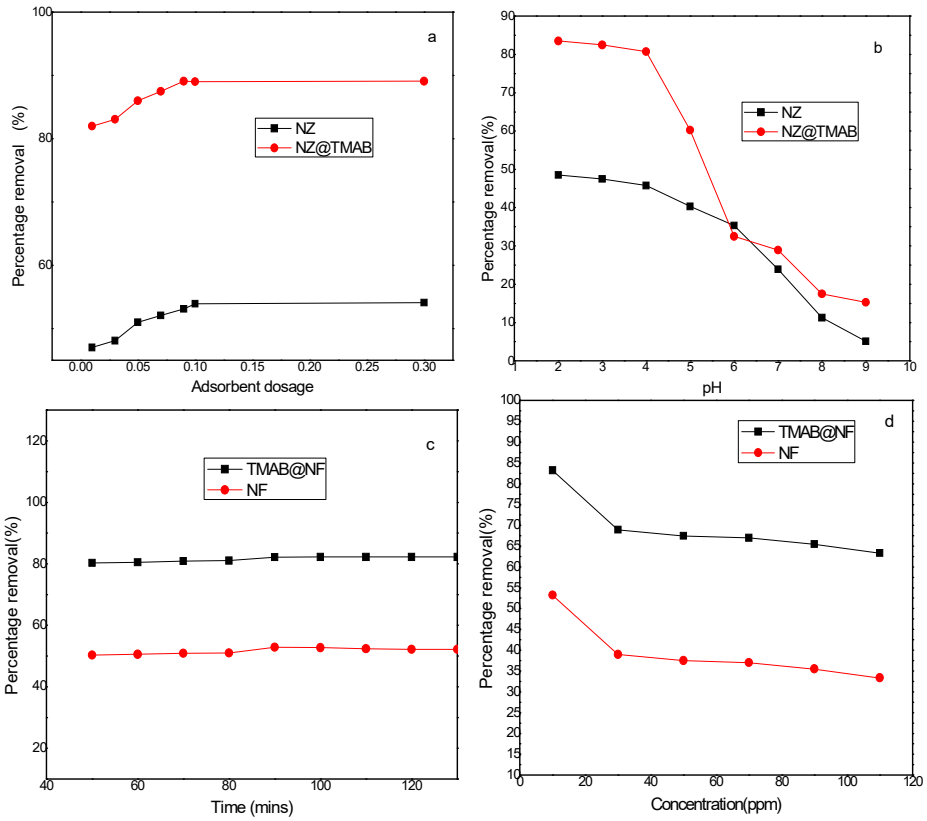

Figure 5. Effect of adsorbent dosage (a), pH (b), time (c) and concentration (d) on the percentage removal of EBT dye by unmodified and TMAB modified $NiFe_2O_4$ nanoparticles.

Effect of pH

The pH values were adjusted between 2 and 9 to compare the effects of pH on the adsorption of EBT dye by unmodified and TMAB-modified $NiFe_2O_4$-NPs. Figure 5b shows the trend of EBT % removal as pH values rise. According to the data, the elimination of EBT reduced as the pH of the solution increased (Figure 5b). The adsorption capacity of EBT at various pHs had been greatly influenced by the zero-point charge (zpc) of $NiFe_2O_4$-NPs. At pH levels lower than pH zpc, $NiFe_2O_4$ NPs' surface retains a positive charge. But at pH zpc, the surface become neutral. However, at pH > pHzpc, a significant negative charge was detected. In this instance, the zeropoint charge of the unaltered $NiFe_2O_4$-NPs keeps a value of 7.5, but after being coated with the TMAB, it shifts to 5.2 as reported in the literature [37].

Therefore, at lower pH levels, the negatively charged dye has been encouraged to bind to the surface of $NiFe_2O_4$-NPs by an acidic medium [38]. Moreover, the delocalization of p-electrons in dye molecules further controls the presence of a negative charge on the surface, which strengthens adsorption at lower pH levels. Yet, the more negative charge that exists on the surface of NPs as a result of the media's basic pH makes EBT dye adsorption even more difficult. Higher pH ranges generate electrostatic repulsion between dye molecules and $NiFe_2O_4$-NP surfaces, which appears to decrease the percentage of dye adsorption. Hence, it was found that pH 2.0 was the most suitable pH for the maximal adsorption of dye molecules. The available charge and aromatic ring structure of the dye molecules have an impact on the adsorption behaviour of EBT dye. The positive charge over the $NiFe_2O_4$-NPs modified by TMAB at pH 2 and the amendable pore size have further impacted the EBT dye's ability to adsorb. The findings suggest that the dye's electrostatic interactions with $NiFe_2O_4$ -NPs with surface modifications are the primary driving force behind efficient adsorptive removal from wastewater samples.

Effect of contact time

In order to determine the dye adsorption equilibration time, the corresponding influence of contact time on EBT elimination percentage was examined. The percentage of dye removal by TMAB@$NiFe_2O_4$-NPs and unmodified was shown in Figure 5c. From the Figure 5c the dye removal reaches a maximum at 50 minutes and after that it remains stable. Thus, the adsorption of dye molecules by TMAB@$NiFe_2O_4$-NPs was due to the numerous sites available on the surface compared to unmodified one. The gradual saturation of the adsorption sites by EBT molecules over time can be used to explain the decline in the percentage of EBT elimination.

Effect of initial dye concentration

The effect of the initial concentrations of EBT on the removal percentage using surface modified $NiFe_2O_4$-NPs was further established by changing the EBT concentration from 10 to 110 mg/L at the fixed pH (2.5) and adsorbent dose (0.05 mg) (Figure 5d). The outcomes have revealed that the removal percentage of EBT by chosen NPs was directly influenced by the initial amount of EBT. There was a linear decrement in the removal percentage of EBT with the increasing initial concentration. This aspect can be explained by the reduction in the ratio of number of available adsorption sites on $NiFe_2O_4$-NPs surface in the presence of higher concentration of dye molecules. The smaller amount of EBT can interact with the surface of $NiFe_2O_4$-NPs more appropriately and efficiently, thus increasing the dye adsorption capacity of $NiFe_2O_4$-NPs.

Adsorption isotherm studies

The linear plots of the isotherm models are used to explain the sorption of EBT dye on TMAB@$NiFe_2O_4$ nanoparticles. To better understand how much adsorbate is adsorbed onto the

surface of a given quantity of both modified and unmodified $NiFe_2O_4$ nanoparticles and to determine which adsorbent has the greatest potential for adsorption. We used the Langmuir, Freundlich, and Temkin isotherms.

$$\frac{1}{q_e} = \frac{1}{K_L q_{max}} . \frac{1}{C_e} + \frac{1}{q_{max}} \quad (3)$$

The values of Langmuir constants are calculated using the above equation [32]. For both TMAB-modified and unmodified $NiFe_2O_4$-NPs, the corresponding plot of C_e/qe versus C_e yields a linear curve. Table 1 lists the calculated values of the Langmuir constants, q_{max} and R^2, for each system.

According to Chung *et al.* [39], the Freundlich isotherm (Eq. (2)) is utilised to explain the nonideal and reversible ability of adsorbate over the surface of a given amount of adsorbent. The nonhomogeneous distribution of adsorption in this model makes multilayer adsorption actually achievable.

$$Log q_e = Log\ K_f + \frac{1}{n}\ Log C_e \quad (4)$$

where K_f (mg/g) is the intercept, and n is the slope of the linear fitting, and their values are derived by plotting Log q_e vs. Log C_e. Table 1 contains the derived values for K_f and n.

$$q_e = \frac{RT}{b_T} \ln A_T + \left(\frac{RT}{b_T}\right) \ln C_e \quad (5)$$

Equation (5) describes how adsorbent, and adsorbate interact in the Temkin isotherm. According to researchers [39], it is noteworthy since it ignores the system's adsorbate concentrations for small and large values. From a linear plot of q_e vs. ln C_e, the values of KT and B1 are determined (Table 1). The isotherm results show that the sorption mechanism of dyes is multilayer adsorption wherein the oxygen functions of TMAB@$NiFe_2O_4$ and EBT dye molecules interact chemically and electrostatically. Few researchers have reported similar outcomes [40, 41]

Table 1. Various parameters calculated from adsorption isotherms.

Isotherms	Parameters	Unmodified $NiFe_2O_4$	TMAB@$NiFe_2O_4$
Langmuir	Slope	0.7826	0.17795
	Q_{max}(mg/g)	40.716	61.8047
	R1	0.3892	0.18030
	R2	0.974	0.98156
Freundlich	Slope	0.67896	0.7187
	kf	5.3797	1.6417
	R2	0.9714	0.99
Temkin	B_1	11.2631	18.5311
	K_T	0.2433	0.6103
	R^2	0.8879	0.8140

Adsorption kinetic studies

The rate of adsorption of the adsorbent is estimated using the adsorption kinetics of EBT dye. But the kinetic investigations are also helpful in figuring out the underlying mechanism that controls the adsorption of EBT dye on the surface of unmodified and TMAB-modified $NiFe_2O_4$ NPs. Pseudo-first-order, pseudo-second order, and intraparticle diffusion models were employed to study the adsorption kinetics of the adsorbed dye on the surface of unmodified and TMAB modified $NiFe_2O_4$ NPs.

The pseudo-first-order kinetic model is given by the following equation 6:

$$Log(q_e - q_t) = Logq_e - \frac{k_1 t}{2.303} \quad (6)$$

where q_e and q_t correspond to the amount of dye adsorbed (mg/g) at equilibrium and the amount of dye adsorbed (mg/g) at time t respectively whereas k1 is for the pseudo-first-order rate constant (min^{-1}) [42]. The slope and intercept of a linear plot of log (q_e-q_t) vs t (minutes) are used to determine the respective values of k_1 and q_e.

The pseudo-second-order kinetic model can be written as Eq.7:

$$\frac{t}{q_t} = \frac{1}{k_2 q_e^2} + \frac{t}{q_e} \quad (7)$$

where q_t is the quantity of adsorbate (in mg/g) that is adsorbed at time t, q_e denotes the quantity of adsorbate (in mg/g) that is adsorbed at equilibrium. The pseudo-second-order rate constant is denoted by k_2, which is expressed as g mg^{-1} min^{-1}. The values of q_e and k_2 are determined from the slope and intercept of a plot of t/q_t vs. t, and the plot is found to be linear.

The rate of transport has been affected by the interaction of the solid ($NiFe_2O_4$-NPs) and diffusion material. The appropriate intraparticle diffusion kinetic model has been used to determine the transport phenomena in order to analyse this behaviour. During this process, species are transferred from the majority of the solution to the solid phase. After analysing the findings, it was found that the correlation coefficient values for the $NiFe_2O_4$ NP for the pseudo-first order, pseudo-second order, and intraparticle diffusion models were, respectively, 0.41, 0.99, and 0.675. The results for TMAB@$NiFe_2O_4$ were 0.806, 0.998, and 0.8655, respectively. For the bare $NiFe_2O_4$ NPs and the TMAB@$NiFe_2O_4$ NPs, the experimental qe value was discovered to be 29.25 and 70.30 mg/g, respectively. The results of the kinetic models lead to the conclusion that the estimated q_e values match the observed qe values derived from the pseudo-second-order kinetic model very well. R^2 results support the pseudo-second-order model's superior fit to the experimental data over the pseudo-first-order model.

Regeneration and reusability of surface modified $NiFe_2O_4$-NPs

In this study, the regeneration of the employed $NiFe_2O_4$ nano adsorbents from the dye solutions was carried out to ensure the suitability of our systems from the standpoint of industrial applications. After being extracted by centrifugation from the dye solutions that had been treated, TMAB modified $NiFe_2O_4$-NPs were washed according to the recommended water-to-ethanol ratio and then dried in an oven to produce $NiFe_2O_4$NPs in powder form. Similar procedures were used for the unmodified $NiFe_2O_4$NPs reusability test. Even after the fourth cycle of reusability, the dye removal percentage using TMAB@$NiFe_2O_4$NPs showed removal of %. Unmodified $NiFe_2O_4$ NPs, however, showed a removal of%. The outcome demonstrated the versatility of $NiFe_2O_4$-NPs. The chemical stability of TMAB@ $NiFe_2O_4$-NPs regained after the application for the fourth cycle further demonstrated its practicability.

Mechanism of EBT adsorption

The interaction of dye molecules with modified and unmodified $NiFe_2O_4$-NPs was found to be best described by the Freundlich model, which was observed from Table 1. A plot illustrating the mechanism of EBT adsorption is given in the Figure 6. A major factor in the EBT adsorption is due to the hydroxyl groups and tetra methyl ammonium ions present on $NiFe_2O_4$ surface. Due to hydrogen bonding and electrostatic attraction, the negative charged dye (EBT) adsorption is facilitated by the TMAB modified adsorbent surface protonation at pH = 2. This surface has a high positive charge density and hence more adsorption of EBT dye. The Freundlich model for TMAB@$NiFe_2O_4$ NPs has the greatest R^2 value of 0.99, confirming the maximal and multilayer

adsorption of EBT molecules on its surface. The reason for higher adsorption on the surface of TMAB@$NiFe_2O_4$ NPs is due to the electrostatic interactions between the negatively charged O atom of EBT and the positively charged N atom of the amine group of TMAB [43]. EBT molecules are layer by layer coated due to the electrostatic interactions on the TMAB@$NiFe_2O_4$-NPs' compared to unmodified. Additionally, by providing more heterogeneous adsorption sites, the nano dimensions of positively charged particles of TMAB@ $NiFe_2O_4$ enhance the adsorption of EBT. The functional groups of the TMAB and dye molecules' bonding properties are actively involved in the improved adsorption of EBT molecules on the surface of the TMAB@ $NiFe_2O_4$ NPs.

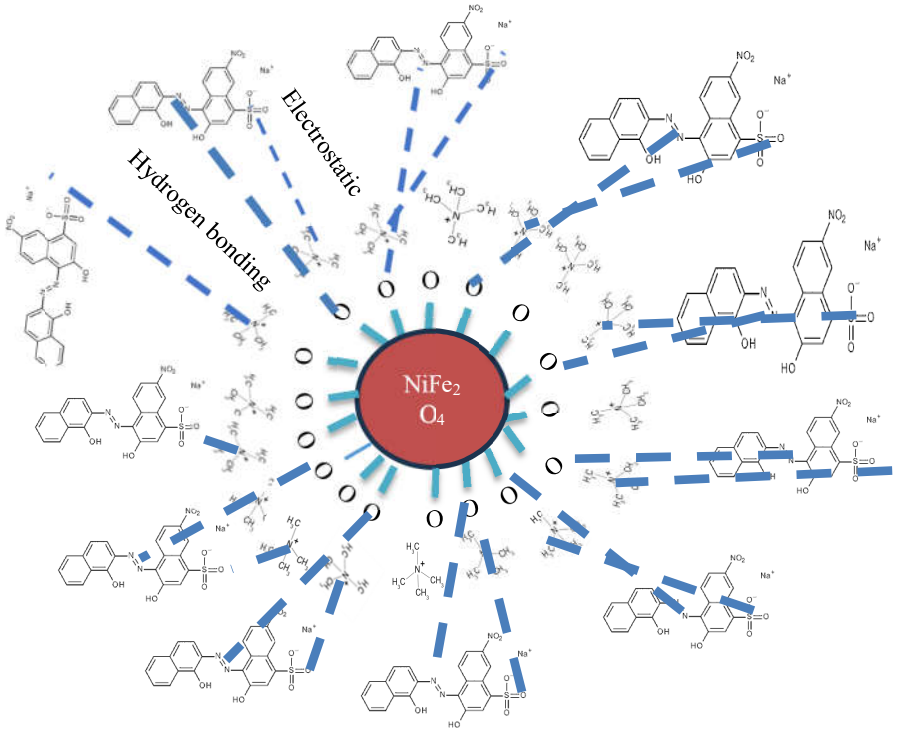

Figure 6. Mechanism of EBT adsorption on TMAB@$NiFe_2O_4$.

CONCLUSION

The easy and simple procedure was successfully used to create the TMAB surface modified $NiFe_2O_4$-NPs, and sophisticated methods including FTIR, XRD, and SEM were used to characterise them. The prospective use of TMAB@$NiFe_2O_4$-NPs for the adsorptive removal of a model anionic dye (EBT dye) was further explored, and they demonstrated a removal rate of 89%, respectively. Utilising surface-modified $NiFe_2O_4$-NPs, the adsorption isotherm examination showed multilayer adsorption of EBT. The EBT elimination was depicted by the adsorption kinetics as a pseudo-second-order model, and the equilibrium data for the adsorption isotherms agrees extremely well with the Freundlich isotherm. The electrostatic interaction between the positively surface-charged $NiFe_2O_4$-NPs and anionic EBT dye provides the electrochemical

interaction between functional groups and dye molecules. Further the reusability experiments confirm the potential practical usage of synthesized TMAB@$NiFe_2O_4$. The results show that the TMAB@$NiFe_2O_4$ has high efficiency for the EBT dye removal from industrial wastewater treatment.

ACKNOWLEDGEMENT

The authors thank KCG College of technology for providing all required facilities to carry out the experiments.

REFERENCES

1. Gómez, V.; Larrechi, M.S.; Callao, M.P. Kinetic and adsorption study of acid dye removal using activated carbon. *Chemosphere* **2007**, 69, 1151-1158.
2. Lakshmipathy, R.; Sarada, N.C. Adsorptive removal of basic cationic dyes from aqueous solution by chemically protonated watermelon (*Citrullus lanatus*) rind biomass. *Desalin. Water Treat*. **2014**, 52, 6175-6184.
3. Dawood, S.; Sen, T.K; Review on dye removal from its aqueous solution into alternative cost effective and non-conventional adsorbents. *J. Chem. Proc. Eng.* **2014**, 1, 1-11.
4. Mahmoodi, N.M.; Abdi, J.; Bastani, D. Direct dyes removal using modified magnetic ferrite nanoparticle. *J. Environ. Health Sci. Eng.* **2014**, 12, 1-10.
5. Andal, V.; Buvaneswari, G. Removal of lead ions by $NiFe_2O_4$ nanoparticles. *IJRET* **2014**, 3, 475-483.
6. Allen, S.J. Types of adsorbent materials-use of adsorbents for the removal of pollutants from wastewaters, CRC: Boca Raton, FL, USA; **1996**; p. 59.
7. Farghali, A.; Bahgat, M.; Elrouby, W.; Khedr, M. Decoration of multiwalled carbon nanotubes (MWCNTs) with different ferrite nanoparticles and its use as an adsorbent. *J. Nano Struc. Chem.* **2013**, 3, 1-13.
8. Jain, A.K.; Gupta, V.K.; Bhatnagar, A.; Suhas; Utilization of industrial waste products as adsorbents for the removal of dyes. *J. Hazard. Mater.* **2003**, 101, 31-42.
9. Pal, B.; Kaur, R.; Grover, I.S. Superior adsorption and photodegradation of Eriochrome Black-T dye by Fe^{3+} and Pt^{4+} impregnated TiO_2 nanostructures of different shapes. *J. Ind. Eng. Chem.* **2016**, 33, 178-184.
10. Mohammed, O.; Mhamed, K.; Houari, M. Synthesis and characterization of activated carbon from asphodelus microcarpus in two steps. *Bull. Chem. Soc. Ethiop.* **2024**, 38, 199-212.
11. Babadi, N.; Tavakkoli1, H.; Afshari, M. Synthesis and characterization of nanocomposite $NiFe_2O_4$@SalenSi and its application in efficient removal of Ni(II) from aqueous solution. *Bull. Chem. Soc. Ethiop.* **2018**, 32, 77-88.
12. Gerçel, Ö.; Gerçel, H.F.; Koparal, A.S.; Öğütveren, Ü.B. Removal of disperse dye from aqueous solution by novel adsorbent prepared from biomass plant material. *J. Hazard. Mater.* **2008**, 160, 668-674.
13. Gunjakar, J.L.; More, A.M.; Gurav, K.V.; Lokhande, C.D. Chemical synthesis of spinel nickel ferrite ($NiFe_2O_4$) nano-sheets. *J. Appl. Surf. Sci.* **2008**, 254, 5844-5848.
14. Salih, S.J.; Mahmood, W.M. Review on magnetic spinel ferrite (MFe_2O_4) nanoparticles: From synthesis to application. *Heliyon* **2023**, 9, e16601.
15. Samson, V.A.F.; Bernadsha, S.B.; Xavier, R.; Rueshwin, C.S.T.; Prathap, S.; Madhavan, J.; Raj, M.V.A. One pot hydrothermal synthesis and characterization of $NiFe_2O_4$ nanoparticles. *Materials Today: Proceedings*, **2022**, 50, 2665-2667.
16. Köseoğlu, Y. Rapid synthesis of nanocrystalline $NiFe_2O_4$ and $CoFe_2O_4$ powders by a microwave-assisted combustion method. *J. Supercond. Nov. Magn.* **2013**, 26, 1391-1396.

17. Hariharasuthan, R; Chitradevi, S; Radha, K.S. Characterization of $NiFe_2O_4$ (nickel ferrite) nanoparticles with very low magnetic saturation synthesized via co-precipitation method. *Appl. Phys. A* **2022**, 128, 1045.
18. Chen, D.-H.; He, X.-R. Synthesis of nickel ferrite nanoparticles by sol-gel method, *Mater. Res. Bull.* **2001**, 36, 1369-1377.
19. Yadav, R.S.; Kuřitka, I.; Vilcakova, J.; Machovsky, M.; Skoda, D.; Urbánek, P.; Masař, M.; Jurča, M.; Urbánek, M.; Kalina, L.; Havlic,a J. $NiFe_2O_4$ nanoparticles synthesized by dextrin from corn-mediated sol-gel combustion method and its polypropylene nanocomposites engineered with reduced graphene oxide for the reduction of electromagnetic pollution. *ACS Omega*. **2019**, 9, 22069-22081.
20. Makofane, A.; Maake, P.J.; Mathipa, M.M.; ; Matinise, N.; ; Cummings, F.R.; Motaung, D.E.; Hintsho-Mbita, N.C. Green synthesis of $NiFe_2O_4$ nanoparticles for the degradation of Methylene Blue, sulfisoxazole and bacterial strains. *Inorg. Chem. Commun*. **2022**, 139, 109348.
21. Shilpa Amulya, M.A.; Nagaswarupa, H.P.; Anil Kumar, M.R.; Ravikumar, C.R.; Prashantha, S.C.; Kusuma, K.B. Sonochemical synthesis of $NiFe_2O_4$ nanoparticles: Characterization and their photocatalytic and electrochemical applications. *Appl. Surf. Sci. Adv.* **2020**, 1, 100023.
22. Liu, X.; Gao, W. Preparation and magnetic properties of $NiFe_2O_4$ nanoparticles by modified Pechini Method. *Mater. Manuf. Process*. **2012**, 27, 905-909.
23. Xu, F.; Zhang, Q.; Gao, Z. Simple one-step synthesis of gold nanoparticles with controlled size using cationic Gemini surfactants as ligands: Effect of the variations in concentrations and tail lengths. *Colloids Surf. A* **2013**, 417, 201-210.
24. Xu, Y.; Zhao, Y.; Chen, L.; Wang, X.; Sun, J.; Wu, H.; Bao, F.; Fan, J.; Zhang, Q. Large-scale, low-cost synthesis of monodispersed gold nanorods using a Gemini surfactant. *Nanoscale* **2015**, 7, 6790-6797.
25. Li, D.; Fang, W.; Feng, Y.; Geng, Q.; Song, M. Stability properties of water-based gold and silver nanofluids stabilized by cationic gemini surfactants. *J. Taiwan Inst. Chem. Eng.* **2019**, 97, 458-465.
26. He, S.; Chen, H.; Guo, Z.; Wang, B.; Tang, C.; Feng, Y. High concentration silver colloid stabilized by a cationic gemini surfactant, *Colloids Surf., A*, **2013**, 429, 98–105.
27. Xu, J.; Han, X.; Liu, H.; Hu, Y. Synthesis and optical properties of silver nanoparticles stabilized by Gemini surfactant. *Colloids Surf. A* **2006**, 273, 179-183.
28. Bhattacharya, S.; Biswas, J. Role of spacer lengths of Gemini surfactants in the synthesis of silver nanorods in micellar media. *Nanoscale* **2011**, 3, 2924.
29. Datta, S.; Biswas, J.; Bhattacharya, S. How does spacer length of imidazolium Gemini surfactants control the fabrication of 2D-Langmuir of silver-nanoparticles at the air-water interface. *J. Colloid Interface Sci*. **2014**, 430, 85-92.
30. Li, D.; Fang, W.; Zhang, Y.; Wang, X.; Guo, M.; Qin, X. Stability and thermal conductivity enhancement of silver nano squids with Gemini surfactants. *Ind. Eng. Chem. Res.* **2017**, 56, 12369-12375.
31. Moeinpour, F.; Alimoradi, A.; Kazemi, M. Efficient removal of Eriochrome black T from aqueous solution using $NiFe_2O_4$ magnetic nanoparticles. *J. Environ. Heal. Sci. Eng*. **2014**, 12, 112.
32. Tahara, L.B.; Oueslati, M.H. Fast adsorption–desorption of Eriochrome Black T using superparamagnetic NiZn ferrite nanoparticles. *Desalin. Water Treat*. **2020**, 196, 315-328.
33. Savić Gajić, I.M.; Savić, I.M.; Svirčev, Z. Preparation and characterization of alginate hydrogels with high water-retaining capacity. *Polymers* **2023**, 15, 2592.
34. Li, D.; Wei, Z.; Xue, C. Alginate-based delivery systems for food bioactive ingredients: An overview of recent advances and future trends. *Compr. Rev. Food Sci. Food Saf*. **2021**, 20, 5345-5369

35. Ramdhan, T.; Ching, S.H.; Prakash, S.; Bhandari, B. Time dependent gelling properties of cuboid alginate gels made by external gelation method: Effects of alginate-$CaCl_2$ solution ratios and pH. *Food Hydrocoll*. **2019**, 90, 232-240.
36. Long, Z.; Zhang, G.; Du, H.; Zhu, J.; Li, J.; Preparation and application of BiOBr-Bi_2S_3 heterojunctions for efficient photocatalytic removal of Cr(VI). *J. Hazard. Mater.* **2021,** 407, 124394.
37. Elfeky, S.A.; Mahmoud, S.E.; Youssef, A.F. Applications of CTAB modified magnetic nanoparticles for removal of chromium(VI) from contaminated water. *J. Adv. Res.* **2017** 8, 435-443.
38. Mansour, A.T.; Alprol, A.E.; Khedawy, M.; Abualnaja, K.M.; Shalaby, T.A.; Rayan, G.; Ramadan, K.M.A.; Ashour, M. Green synthesis of zinc oxide nanoparticles using red seaweed for the elimination of organic toxic dye from an aqueous solution. *Materials (Basel)* **2022**, 15, 5169.
39. Kaur, Y. Bhatia, Y.; Chaudhary, S.; Chaudhary, G.R. Comparative performance of bare and functionalize ZnO nanoadsorbents for pesticide removal from aqueous solution. *J. Mol. Liq*. **2017**, 234, 94-103.
40. Afkhami, A.; Moosavi, R. Adsorptive removal of Congo red, a carcinogenic textile dye, from aqueous solutions by maghemite nanoparticles. *J. Hazard. Mater.* **2010**, 174, 398-403.
41. Mittal, A.; Kurup, L.; Mittal, J. Freundlich and Langmuir adsorption isotherms and kinetics for the removal of tartrazine from aqueous solutions using hen feathers. *J. Hazard. Mater.* **2007**, 146, 243-248.
42. Chung, H.K.; Kim, W.H.; Park, J.; Cho, J.; Jeong, T.Y.; Park, P.K. Application of Langmuir and Freundlich isotherms to predict adsorbate removal efficiency or required amount of adsorbent. *J. Ind. Eng. Chem.* **2015**, 28, 241-246.
43. Luna, M.D.G.; Edgar, D.F. Divine, A.D.G.; Cybelle, M.F.; Meng, W.W. Adsorption of Eriochrome Black T (EBT) dye using activated carbon prepared from waste rice hulls—Optimization, isotherm and kinetic studies. *J. Taiwan Inst. Chem. Eng*. **2013**, 44, 646-653.